

ISSN: (Print) (Online) Journal homepage: <https://www.tandfonline.com/loi/ktib20>

# A host–gut microbial amino acid co-metabolite, *p*-cresol glucuronide, promotes blood–brain barrier integrity *in vivo*

Andrew V. Stachulski, Tobias B-A Knausenberger, Sita N. Shah, Lesley Hoyles & Simon McArthur

To cite this article: Andrew V. Stachulski, Tobias B-A Knausenberger, Sita N. Shah, Lesley Hoyles & Simon McArthur (2022): A host–gut microbial amino acid co-metabolite, *p*-cresol glucuronide, promotes blood–brain barrier integrity *in vivo*, Tissue Barriers, DOI: [10.1080/21688370.2022.2073175](https://doi.org/10.1080/21688370.2022.2073175)

To link to this article: <https://doi.org/10.1080/21688370.2022.2073175>



© 2022 The Author(s). Published with license by Taylor & Francis Group, LLC.



View supplementary material [↗](#)



Published online: 20 May 2022.



Submit your article to this journal [↗](#)



View related articles [↗](#)



View Crossmark data [↗](#)

# A host–gut microbial amino acid co-metabolite, *p*-cresol glucuronide, promotes blood–brain barrier integrity *in vivo*

Andrew V. Stachulski<sup>a</sup>, Tobias B-A Knausenberger<sup>b</sup>, Sita N. Shah<sup>b</sup>, Lesley Hoyles<sup>c</sup>, and Simon McArthur<sup>b</sup> 

<sup>a</sup>Department of Chemistry, Robert Robinson Laboratories, University of Liverpool, Liverpool, UK; <sup>b</sup>Institute of Dentistry, Faculty of Medicine & Dentistry, Queen Mary, University of London, Blizard Institute, London, UK; <sup>c</sup>Department of Bioscience, School of Science and Technology, Nottingham Trent University, Clifton, Nottingham, UK

## ABSTRACT

The sequential activity of gut microbial and host processes can exert a powerful modulatory influence on dietary components, as exemplified by the metabolism of the amino acids tyrosine and phenylalanine to *p*-cresol by gut microbes, and then to *p*-cresol glucuronide (pCG) by host enzymes. Although such glucuronide conjugates are classically thought to be biologically inert, there is accumulating evidence that this may not always be the case. We investigated the activity of pCG, studying its interactions with the cerebral vasculature and the brain *in vitro* and *in vivo*. Male C57Bl/6 J mice were used to assess blood–brain barrier (BBB) permeability and whole-brain transcriptomic changes in response to pCG treatment. Effects were then further explored using the human cerebromicrovascular endothelial cell line hCMEC/D3, assessing paracellular permeability, transendothelial electrical resistance and barrier protein expression. Mice exposed to pCG showed reduced BBB permeability and significant changes in whole-brain transcriptome expression. Surprisingly, treatment of hCMEC/D3 cells with pCG had no notable effects until co-administered with bacterial lipopolysaccharide, at which point it was able to prevent the permeabilizing effects of endotoxin. Further analysis suggested that pCG acts as an antagonist at the principal lipopolysaccharide receptor TLR4. The amino acid phase II metabolic product pCG is biologically active at the BBB, antagonizing the effects of constitutively circulating lipopolysaccharide. These data add to the growing literature showing glucuronide conjugates to be more than merely metabolic waste products and highlight the complexity of gut microbe to host communication pathways underlying the gut–brain axis.

## ARTICLE HISTORY

Received 7 February 2022  
Revised 28 April 2022  
Accepted 28 April 2022

## KEYWORDS

Blood–brain barrier; gut–brain axis; gut microbiota; glucuronidation


## Introduction

The gut microbiota can influence a wide range of physiological systems and pathological conditions, ranging from cardiovascular function<sup>1</sup> to metabolic disease<sup>2</sup> to cancer,<sup>3</sup> but communication between the gut microbiota and the brain is one of the most active areas of investigation. Interactions between the gut microbes and the brain have been identified in both cognitive functions such as anxiety<sup>4</sup> and sociability,<sup>5</sup> and in overt disease states including Parkinson's disease,<sup>6</sup> multiple sclerosis<sup>7</sup> and dementia.<sup>8</sup> Increasingly, evidence indicates a central role for microbe-derived metabolites in this dialogue, acting primarily through three routes: directly on enteric and gut extrinsic neural pathways, by modification of enteroendocrine signaling

or, as we and others have shown, via the circulation and interactions with the blood–brain barrier (BBB).<sup>9,10</sup> Notably, while many microbe-derived metabolites circulate in their native form, many others are subjected to host metabolic enzyme-mediated biotransformation, thereby altering their biological activities.

A good example of this lies in the metabolism of the microbial product *p*-cresol (4-methylphenol). This molecule is produced by bacterial fermentation of dietary tyrosine and phenylalanine in the colon,<sup>11</sup> and passes through the gut epithelium into the portal vasculature. Notably, *p*-cresol undergoes extensive conjugation both in enterocytes<sup>12</sup> and by hepatic enzymes upon reaching the liver,<sup>13</sup> such that the parent compound is essentially not found

**CONTACT** Lesley Hoyles  [lesley.hoyles@ntu.ac.uk](mailto:lesley.hoyles@ntu.ac.uk)  Department of Bioscience, School of Science and Technology, Nottingham Trent University, Clifton, Nottingham, UK; CONTACT Simon McArthur  [s.mcarthur@qmul.ac.uk](mailto:s.mcarthur@qmul.ac.uk)  Institute of Dentistry, Faculty of Medicine & Dentistry, Queen Mary, University of London, Blizard Institute, 4, Newark Street, London E1 2AT, UK; Andrew V. Stachulski  [stachuls@liverpool.ac.uk](mailto:stachuls@liverpool.ac.uk)  Department of Chemistry, Robert Robinson Laboratories, University of Liverpool, Liverpool L69 7ZD, UK

 Supplemental data for this article can be accessed online at <https://doi.org/10.1080/21688370.2022.2073175>

© 2022 The Author(s). Published with license by Taylor & Francis Group, LLC.

This is an Open Access article distributed under the terms of the Creative Commons Attribution-NonCommercial-NoDerivatives License (<http://creativecommons.org/licenses/by-nc-nd/4.0/>), which permits non-commercial re-use, distribution, and reproduction in any medium, provided the original work is properly cited, and is not altered, transformed, or built upon in any way.

within the systemic circulation,<sup>14</sup> existing rather as *p*-cresol sulfate (pCS) with a smaller component as *p*-cresol glucuronide (pCG).<sup>15,16</sup> While pCS has been extensively studied in light of its role as a major uremic toxin,<sup>15</sup> the potential biological actions of pCG have received far less attention, although high concentrations of the metabolite have been shown to potentiate pCS-induced neutrophil oxidative burst activity *in vitro*<sup>17</sup> and to slightly raise fasting glycemia in mice.<sup>18</sup> What role the molecule might play at more physiologically representative concentrations is unclear.

Classically, glucuronidation is considered as part of the phase II metabolic pathways, with the actions of the numerous UDP-glucuronosyltransferases serving to enhance renal clearance of parent compounds.<sup>19</sup> More recent evidence suggests that this form of conjugation may not always be a neutralizing process however. Notably, glucuronide derivatives of morphine, ethanol and estradiol have been shown to act as agonists of the Toll-like receptor 4 (TLR4) complex, promoting allodynia and inflammation upon spinal cord administration,<sup>20–23</sup> actions quite distinct from those of their parent compounds, and highlighting the potential of glucuronide conjugates to gain potentially significant new pharmacological activity. Whether the same can be said for microbe-derived compounds present in the circulation is unclear, with studies into this question hindered by difficulties in obtaining pure molecules for study. We have recently established a novel pathway for chemical synthesis of pCG,<sup>24</sup> and here we employ a combined *in vitro/in vivo* approach to identify the actions of this compound on the cerebral vasculature and the brain.

## Materials and methods

### Drugs and reagents

Trimethylsilyl trifluoromethanesulfonate was purchased from Fluorochem Ltd. UK and methyl 1,2,3,4-*tetra-O*-acetyl- $\beta$ -D-glucuronate from Carbosynth UK. Solvents were of minimum HPLC grade and were purchased from Fisher Scientific, UK. Ultrapure lipopolysaccharide (LPS) from *Porphyromonas gingivalis* was purchased from InvivoGen (Toulouse, France). Evans blue,

70 kDa FITC-dextran and MTT (3-(4,5-dimethylthiazol-2-yl)-2,5-diphenyltetrazolium bromide) were purchased from Merck Life Science UK Ltd., UK.

### Animals

Wild-type male C57Bl/6 J mice aged between 7 and 8 weeks (Charles River UK Ltd., Margate, UK) were used for all experiments. Mice were kept under a 12 h:12 h light:dark regime, with *ad libitum* access to standard chow (Envigo Ltd., UK) and drinking water; all animals were acclimatized to the holding facility environment for 1 week prior to experimentation. Animals were treated as described below and killed by transcardial perfusion with ice-cold saline under pentobarbitone anesthesia. All experiments were approved by the QMUL Animal Welfare and Ethical Review Board and were performed in accordance with the ethical standards laid down in the 1964 Declaration of Helsinki and its later amendments and with the UK Animals (Scientific Procedures) Act, 1986, under Project License PFA5C4F4F.

### *In vivo* BBB permeability analysis

Mice ( $n = 5–6$  per group) were injected i.p. with 1 mg/kg body weight pCG in 100  $\mu$ l saline vehicle, a dose calculated to approximately double circulating concentrations,<sup>18</sup> followed 2 h or 6 h later by assessment of Evans blue extravasation. One hour before assessment animals were injected i.p. with 100  $\mu$ l of a 2% (w/v) solution of Evans blue dye in 0.9% saline. Dye was permitted to circulate for 1 h before animals were transcardially perfused with 0.9% saline at 4°C to remove dye remaining in the vasculature. Blood samples were allowed to coagulate at 37°C for 15 minutes prior to centrifugation at 800 g for 10 minutes to separate serum. Brains were removed and homogenized by maceration in 0.1 M phosphate-buffered saline. Suspended macromolecules were precipitated by incubation with 60% trichloroacetic acid, and dye content of resulting supernatants was detected using a CLARIOstar spectrophotometer (BMG Labtech GmbH, Germany) alongside a standard curve of defined concentrations of Evans blue in the same

buffer. Brain Evans' blue content was expressed as  $\mu\text{g}$  of dye per  $\text{mg}$  of brain tissue, normalized to circulating serum concentrations.

### **RNAseq data analyses**

Processing of mouse brain samples (taken at 2 h) and RNA extraction were performed as described previously.<sup>10</sup> RNA samples ( $n = 6$  pCG,  $n = 6$  control) were sent to MacroGen Inc. (Seoul, Republic of Korea) where they were subject to quality checks (RIN analysis); libraries were prepared (TruSeq Stranded mRNA LT Sample Prep Kit) for paired-end ( $2 \times 100$  nt) sequencing on an Illumina HiSeq 4000 apparatus. Three pCG-treated and three saline controls produced data of poor quality so were excluded from analyses after quality checks and consideration of MacroGen quality reports; as such, samples SG1, SG3, SG5, CG2, CG5 and CG6 were used for all analyses described from hereon. Raw RNAseq (fastq) sequence data were processed in house as described previously.<sup>10</sup> Entrez gene identifiers were converted to gene symbols using *Mus musculus* annotations downloaded from NCBI on 4 January 2021; only those genes with valid Entrez gene identifiers were retained in analyses. Significantly differentially expressed genes (FDR  $P < .05$ ) identified using DESeq2 v1.22.1<sup>25</sup> were analyzed by mouse KEGG pathway over-representation analysis using Enrichr<sup>26,27</sup> and manual curation. Signaling Pathway Impact Analysis (SPIA v1.22.1)<sup>28</sup> was used to determine whether Kyoto Encyclopedia of Genes and Genomes (KEGG) *Mus musculus* pathways (downloaded on 22 December 2021) were activated or inhibited in mouse brain cells exposed to pCG. RNAseq data have been deposited in ArrayExpress under accession number E-MTAB-11340. Normalized and  $\log_2$ -transformed RNAseq data are available as Supplementary Material (Suppl. Table 1).

### **Cell culture**

The human cerebrovascular endothelial cell line hCMEC/D3 was maintained and treated as described previously.<sup>29</sup> Cells were cultured to confluency in complete endothelial cell growth medium MV2 (PromoCell GmbH, Germany), whereupon VEGF was removed and cells were

further cultured for a minimum of 4 d to enable intercellular tight junction formation prior to experimentation. All cell cultures were used between passages 28 and 32 to ensure retention of appropriate endothelial characteristics.<sup>30</sup>

### **Cell survival analysis**

The potential for pCG-induced cytotoxicity was assessed using the MTT assay. Briefly, cells were treated with pCG for 24 h (0.1, 1, 10, 100  $\mu\text{M}$ ), prior to administration of MTT at 500  $\mu\text{g}/\text{ml}$ . Cells were incubated at 37°C for 2 h, medium was removed and resulting crystals were solubilized by incubation for 2 minutes in dimethyl sulfoxide. Absorbance was read at 540 nm using a CLARIOstar spectrophotometer (BMG Labtech, Ortenberg, Germany), with a reference wavelength at 570 nm.

### **In vitro barrier function assessments**

Paracellular permeability and transendothelial electrical resistance were measured on 100% confluent cultures polarized by growth on 24-well plate polyethylene terephthalate (PET) transwell inserts (surface area: 0.33  $\text{cm}^2$ , pore size: 0.4  $\mu\text{m}$ ; Appleton Woods, UK) previously coated with calf-skin collagen (15  $\mu\text{g}/\text{cm}^2$  and fibronectin 3  $\mu\text{g}/\text{cm}^2$ ; both Merck Life Science UK Ltd.). The permeability of hCMEC/D3 cell monolayers to 70 kDa FITC-dextran (2 mg/ml) was measured as described previously.<sup>31,32</sup> Transendothelial electrical resistance (TEER) measurements were performed using a Millicell ERS-2 Voltohmmeter (Millipore, Watford, UK) and were expressed as  $\Omega \cdot \text{cm}^2$ . In all cases, values obtained from cell-free inserts similarly coated with collagen and fibronectin were subtracted from the total values.

### **Immunofluorescence**

Confluent hCMEC/D3 monolayers grown on transwell inserts as described above were fixed by immersion in 2% formaldehyde in 0.1 M PBS for 10 minutes at room temperature. Cells were immunostained according to standard protocols<sup>33</sup> using a primary rabbit anti-human antibody directed against zona occludens-1 (ZO-1; 1:100, Thermo

Fisher Scientific, UK) and a AF488-conjugated secondary goat anti-rabbit antibody (1:500, Thermo Fisher Scientific, UK) or AF488-conjugated phalloidin (100 nM; Cytoskeleton Inc., Denver, USA). Nuclei were counterstained with DAPI (50 ng/ml; Merck Life Science UK Ltd., UK). Images were captured using an LSM880 confocal laser scanning microscope (Carl Zeiss Ltd., Cambridge, UK) fitted with 405 nm and 488 nm lasers and a 63x oil immersion objective lens (NA, 1.4 mm, working distance, 0.17 mm). Images were captured with ZEN imaging software (Carl Zeiss Ltd., UK) and analyzed using ImageJ 1.53c (National Institutes of Health, USA).

### Flow cytometry

Cells were labeled with APC-conjugated mouse monoclonal anti-CD11b (BioLegend, UK), FITC-conjugated mouse monoclonal anti-CD14 (BioLegend, UK), FITC-conjugated mouse monoclonal anti-MD2 (BioLegend, UK), PE-conjugated mouse monoclonal anti-TLR4, APC-conjugated mouse monoclonal anti-BCRP (BD Biosciences, Oxford, UK), or PE-conjugated mouse monoclonal anti-MDR1A (BD Biosciences, UK), for analysis by flow cytometry. Briefly, cells were treated as described below and, in the case of hCMEC/D3 cells, detached using 0.05% trypsin and incubated with antibodies for 20 minutes at 4°C. Fluorescence was analyzed for 10,000 events per treatment using a BD FACS Canto II flow cytometer (BD Biosciences, UK), and data were analyzed using FlowJo 8.0 software (Treestar Inc., CA, USA).

### Western blot

Samples boiled in 6x Laemmli buffer were subjected to standard SDS-PAGE (10%) and electrophoretically blotted onto Immobilon-P polyvinylidene difluoride membranes (Merck Millipore, Ltd., UK). Membranes were probed using antibodies raised against human occludin (rabbit polyclonal, 1:250, Thermo Fisher Scientific, UK) or  $\beta$ -actin (mouse monoclonal, 1:3000, Merck UK) in Tris-buffer saline solution containing 5% bovine serum albumin overnight at 4°C. Membranes were washed with Tris-buffer saline solution containing 0.1% Tween-20 and incubated with secondary antibody (horseradish

peroxidase-conjugated goat anti-rabbit or anti-mouse, 1:5000; Thermo Fisher Scientific, UK) for 1 hour at room temperature. Proteins were then detected using enhanced chemiluminescence detection (2.5 mM luminol, 0.4 mM p-coumaric acid, 7.56 mM H<sub>2</sub>O<sub>2</sub> in 0.1 M Tris, pH 8.5) and visualized using a ChemiDoc MP Imaging System (Bio-Rad Laboratories Ltd., UK). Integrated optical densities were calculated using NIH ImageJ 1.53c (National Institutes of Health, USA), and ratios of occludin or claudin-5 to  $\beta$ -actin were compared.

### Efflux transporter assays

Activity of the major efflux transporters P-glycoprotein and BCRP was determined using commercially available assays (PREDEASY™ ATPase Assay Kits, Solvo Biotechnology Inc., Budapest, Hungary), performed according to the manufacturer's instructions. Stepwise dose-response curves centered around reported physiological circulating concentrations of pCG (12.3 nM–27  $\mu$ M) were constructed ( $n = 4$ ) to investigate stimulatory and inhibitory effects upon transporter activity.

### Statistical analysis

Sample sizes were calculated to detect differences of 15% or more with a power of 0.85 and  $\alpha$  set at 5%, calculations being informed by previously published data.<sup>10,29</sup> Experimental data are expressed as mean  $\pm$  SEM, with  $n = 6$ –9 independent experiments for all studies. In all cases, normality of distribution was established using the Shapiro–Wilk test, followed by analysis with two-tailed Student's *t*-tests to compare two groups or, for multiple comparison analysis, one- or two-way ANOVA followed by *post hoc* analysis by either Dunnett's test (for dose-response experiments) or Tukey's HSD test (all other comparisons). A *P* value of less than or equal to 5% was considered significant.

## Results

### Synthesis of *p*-cresol glucuronide

As previously described<sup>24</sup> and shown schematically (Figure 1a), reaction of *p*-cresol **1** with 1,2,3,4-tetra-*O*-acetyl- $\beta$ -D-glucuronate **2** in CH<sub>2</sub>Cl<sub>2</sub> promoted



by trimethylsilyl trifluoromethanesulfonate afforded the conjugate **3** in very good yield as a single  $\beta$ -anomer. Hydrolysis of **3** under mild conditions (aq.  $\text{Na}_2\text{CO}_3$ , MeOH) afforded the desired glucuronide sodium salt **4** after partial neutralization to pH 6. Recrystallization gave material of microanalytical purity, as indicated by the  $^1\text{H}$  NMR spectrum (Figure 1b).

### pCG modulates BBB integrity and the whole-brain transcriptome *in vivo*

A defining property of the cerebral vasculature is the existence of a tight barrier function limiting passage of soluble molecules into the brain parenchyma, the BBB. We examined whether exposure

to increased levels of pCG could affect BBB integrity *in vivo*, assessed by monitoring extravasation of administered Evans blue dye into the brain tissue. Treatment of mice with 1 mg/kg pCG i.p. (a dose known to approximately double baseline serum concentrations<sup>18</sup>) caused a significant reduction in entry of Evans blue to the brain tissue, by approximately 50% within 6 h of treatment (Figure 2a).

To investigate the mechanism(s) underlying this action of pCG, we performed bulk RNAseq analysis of brain tissue from animals treated for 2 h with 1 mg/kg pCG i.p., identifying 7702 significantly differentially expressed genes (Figure 2b; Suppl. Table 2), of which 1658 and 1433 showed greater than twofold up- or down-regulation respectively following correction for

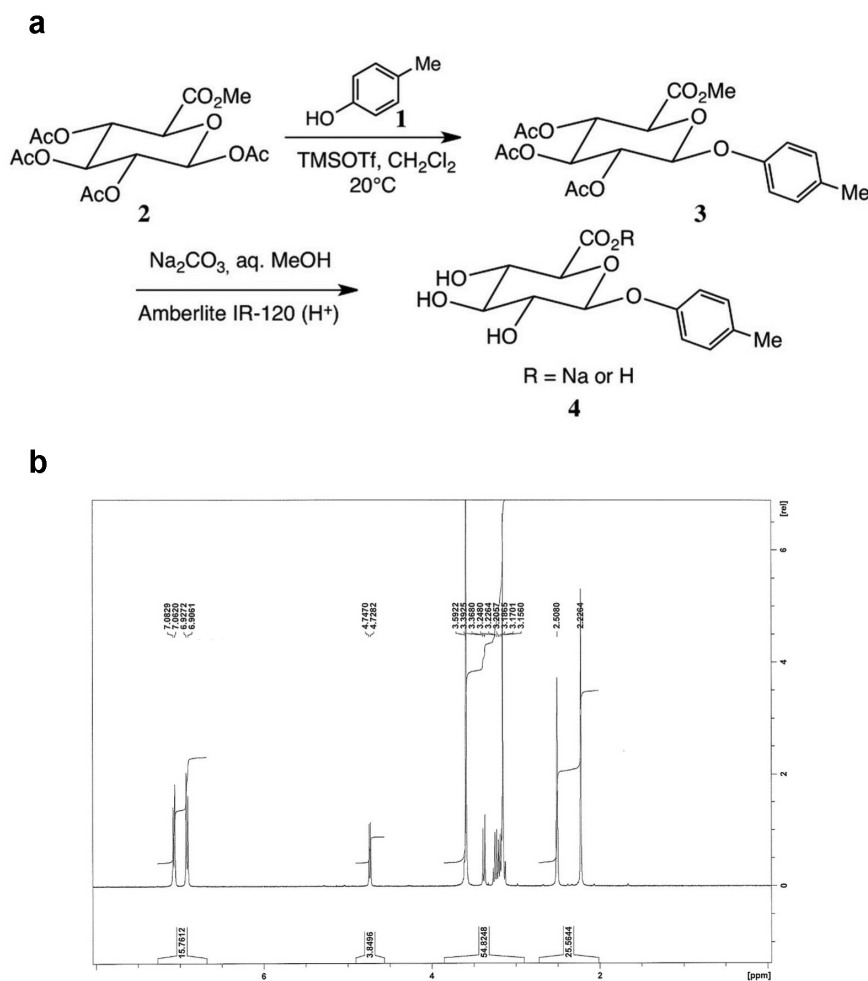


**Figure 1. Production and validation of pCG.** (a) Schematic synthetic pathway for the production of pCG, as previously reported<sup>24</sup>: (1) 4-methylphenol (or *p*-cresol), (2) methyl 1,2,3,4-*tetra-O*-acetyl  $\beta$ -D-glucopyranosiduronate, (3) methyl 1-(4-methylphenyl)-2,3,4-tri-*O*-acetyl- $\beta$ -D-glucopyranosiduronate, (4) (4-methylphenyl)- $\beta$ -D-glucopyranosiduronic acid, sodium salt. (b) Typical  $^1\text{H}$ -NMR spectroscopy trace indicating microanalytical purity of *de novo* synthesized pCG.

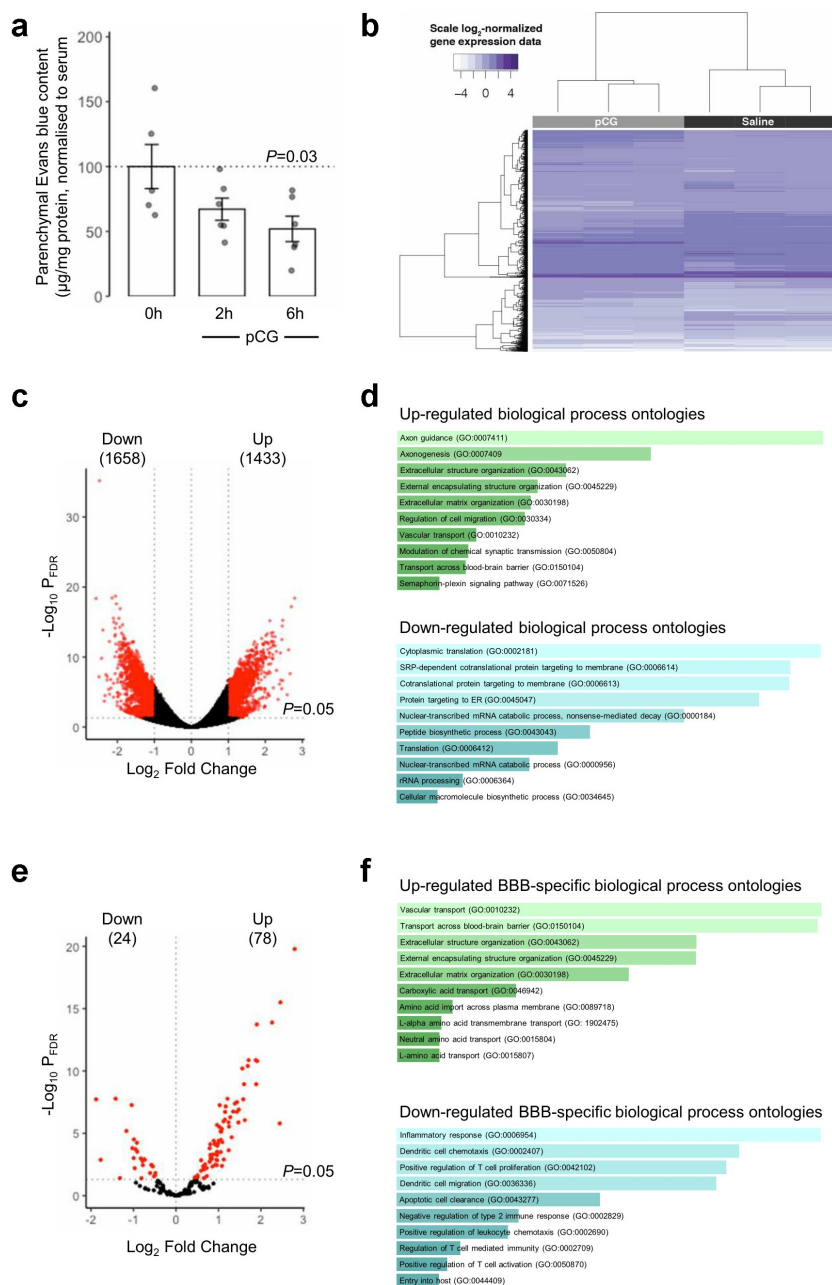


**Figure 2. pCG treatment alters murine BBB permeability and central nervous system (CNS) transcriptional profile *in vivo*.** (a) Treatment of male C57Bl/6 mice by i.p. injection of pCG (1 mg/kg) caused a time-dependent reduction in extravasation of Evans blue tracer into the CNS parenchyma, reaching statistical significance 6 h post administration; data are mean  $\pm$  s.e.m. ( $n = 6$ ). (b) Heatmap showing expression of the 7702 genes found to be significantly ( $P_{FDR} < 0.05$ ) differentially expressed in the CNS of male C57Bl/6 mice 2 h following i.p. injection of 1 mg/kg pCG ( $n = 3$  per group). (c) Volcano plot showing 3091 significantly ( $P_{FDR} < 0.05$ ) twofold differentially expressed genes (red dots). (d) Biological processes associated with genes found to be significantly and  $\geq 2$ -fold upregulated ( $n = 1433$ ) or downregulated ( $n = 1658$ ) upon exposure of mice to pCG. Images are based on Enrichr  $P$  value ranking from GO analysis, the lighter the color and longer the bar, the more is significant is the result, as determined by rank-based ranking; only the top ten results are shown in each case. (e) Volcano plot showing significantly ( $P_{FDR} < 0.05$ ) differentially expressed BBB-relevant genes (red dots). (f) Biological processes associated with BBB-relevant genes found to be significantly upregulated ( $n = 78$ ) or downregulated ( $n = 24$ ) upon exposure of mice to pCG. Images are based on Enrichr  $P$  value ranking from GO analysis, the lighter the color and longer the bar, the more is significant is the result, as determined by rank-based ranking; only the top ten results are shown in each case.

multiple testing (Figure 2c). Analysis of gene ontology categories over-represented within these gene sets using Enrichr<sup>26,27,34</sup> identified a number of different biological process ontologies exhibiting significant changes (Figure 2d), with ontologies relating to axon generation and extracellular matrix organization being notably upregulated, while pathways associated with protein synthesis and ribosomal activity were downregulated. SPIA of all differentially expressed genes revealed several significantly over-represented KEGG pathways (Suppl. Figure 2a), notably indicating pathways associated with growth factor/transcription factor signaling and the response to infection as being activated, while pathways associated with cellular degradation and metabolism were inhibited (Suppl. Figure 2b).

To specifically examine the interactions of pCG with the BBB, we further interrogated transcriptomic changes induced by pCG treatment by comparison with a defined list of 203 known BBB-relevant genes,<sup>29</sup> identifying a total of 78 upregulated and 24 downregulated number of genes exhibiting statistically significant regulation (Figure 2e; Suppl. Table 3). Examination of associated biological process gene ontologies here identified clear upregulation in multiple transport pathways and suppression of inflammatory processes (Figure 2f). Individual gene-level analysis of differentially expressed transporter systems identified enhanced expression of a wide range of nutrient uptake transporters, whereas in contrast only the transporters for myo-inositol and transferrin and aquaporin-4 were significantly downregulated (Table 1).

### **pCG has limited direct effects upon an *in vitro* model of the BBB**

Following these *in silico* analyses, we sought to investigate the biological pathway(s) through which pCG affected the BBB, using a well-established model of the human brain capillary endothelium, the hCMEC/D3 cell line.<sup>35</sup> Initial assessment of potential pCG toxicity using the MTT assay showed no effects on cell survival following 24 h treatment of hCMEC/D3 cells with concentrations of up to 100  $\mu$ M pCG (Figure 3a). Similarly, as  $\beta$ -glucuronidase is known to be present in the

cerebral endothelium, albeit at low levels,<sup>36</sup> it is plausible that the effects of pCG may be caused by reversion to its parent *p*-cresol molecule. However, exposure of hCMEC/D3 cells to *p*-cresol itself (5  $\mu$ M, 24 h) caused a significant increase in paracellular permeability to a 70 kDa FITC-dextran tracer and accompanying reduction in transendothelial electrical resistance (Suppl. Figure 1), indicating an abrogation of BBB integrity, essentially the opposite of our *in vivo* findings.

We then examined the ability of pCG itself to affect hCMEC/D3 monolayer barrier integrity. Exposure of hCMEC/D3 cells for 24 h to pCG caused a dose-dependent increase in transendothelial electrical resistance, becoming statistically significant with 10  $\mu$ M and 100  $\mu$ M concentrations (Figure 3b), but this was not accompanied by any change in permeability to the 70 kDa FITC-dextran tracer (Figure 3c). Microscopic examination of the tight junction component ZO-1 and the actin cytoskeleton to which it binds similarly revealed little effect of pCG upon the endothelial cells (Figure 3d). Similarly, pCG treatment had no effect on the expression of the key tight junction molecule, occludin (Figure 3e-f).

As our transcriptomic data indicated upregulation of multiple nutrient uptake transporter genes, we investigated whether pCG could also affect two of the principal efflux transport systems of the BBB, namely P-glycoprotein and Breast Cancer Resistance Protein (BCRP). While pCG had no effect on cell surface P-glycoprotein expression at any dose tested (Figure 3g), exposure of cells to 100  $\mu$ M pCG did cause a slight, but significant reduction in BCRP expression (Figure 3j). Neither transporter was activated or inhibited by the presence of pCG at any concentrations tested (Figure 3h-i, k-l).

### **pCG antagonizes the BBB-permeabilizing actions of bacterial LPS**

In light of the contrast between the limited effects of pCG seen in our *in vitro* BBB model, we sought alternative explanations for the more pronounced effects of the metabolite seen *in vivo*, taking a lead from the indicated suppression of inflammatory process ontologies. Several structurally dissimilar glucuronidated molecules interact with the



**Table 1.** Significantly differentially expressed BBB-associated transporter genes following pCG treatment *in vivo*.

Gene	Name	Saline	pCG	Direction	P <sub>FDR</sub>
<i>Ldlr</i>	Low-density lipoprotein receptor	6.91 ± 0.32	8.67 ± 0.42	Up	3.98 × 10 <sup>-11</sup>
<i>Abca2</i>	ATP binding cassette subfamily A member 2	10.49 ± 0.77	12.61 ± 0.42	Up	1.15 × 10 <sup>-9</sup>
<i>Slc2a1</i>	Solute carrier family 2 member 1	9.95 ± 0.48	11.66 ± 0.35	Up	1.15 × 10 <sup>-9</sup>
<i>Slc38a3</i>	Solute carrier family 38 member 3	9.36 ± 0.47	10.84 ± 0.32	Up	4.15 × 10 <sup>-8</sup>
<i>Slc1a4</i>	Solute carrier family 1 member 4	9.28 ± 0.21	10.48 ± 0.28	Up	6.98 × 10 <sup>-8</sup>
<i>Slc7a5</i>	Solute carrier family 7 member 5	8.94 ± 0.6	10.55 ± 0.37	Up	1.26 × 10 <sup>-7</sup>
<i>Slc6a9</i>	Solute carrier family 6 member 9	8.40 ± 0.63	9.98 ± 0.32	Up	1.92 × 10 <sup>-7</sup>
<i>Slc7a1</i>	Solute carrier family 7 member 1	8.54 ± 0.34	9.75 ± 0.28	Up	8.06 × 10 <sup>-7</sup>
<i>Slc38a5</i>	Solute carrier family 38 member 5	4.61 ± 0.5	6.42 ± 0.23	Up	8.78 × 10 <sup>-7</sup>
<i>Slc27a4</i>	Solute carrier family 27 member 4	9.73 ± 0.27	10.88 ± 0.31	Up	1.10 × 10 <sup>-6</sup>
<i>Slc16a2</i>	Solute carrier family 16 member 2	8.35 ± 0.34	9.62 ± 0.44	Up	1.30 × 10 <sup>-6</sup>
<i>Slc22a8</i>	Solute carrier family 22 member 8	7.65 ± 0.37	8.77 ± 0.21	Up	7.13 × 10 <sup>-6</sup>
<i>Slc29a4</i>	Solute carrier family 29 member 4	7.01 ± 0.73	8.50 ± 0.45	Up	2.09 × 10 <sup>-5</sup>
<i>Mfsd2a</i>	Major facilitator superfamily domain containing 2A	8.51 ± 0.48	9.57 ± 0.21	Up	9.88 × 10 <sup>-5</sup>
<i>Slc38a1</i>	Solute carrier family 38 member 1	10.63 ± 0.27	11.46 ± 0.11	Up	1.60 × 10 <sup>-4</sup>
<i>Abcc4</i>	ATP binding cassette subfamily C member 4	7.20 ± 0.31	8.20 ± 0.49	Up	3.25 × 10 <sup>-4</sup>
<i>Slco2b1</i>	Solute carrier organic anion transporter family member 2B1	7.93 ± 0.62	9.02 ± 0.22	Up	3.28 × 10 <sup>-4</sup>
<i>Slc27a1</i>	Solute carrier family 27 member 1	9.77 ± 0.53	10.74 ± 0.15	Up	5.02 × 10 <sup>-4</sup>
<i>Abcc1</i>	ATP binding cassette subfamily C member 1	8.00 ± 0.44	8.90 ± 0.25	Up	8.66 × 10 <sup>-4</sup>
<i>Slc5a6</i>	Solute carrier family 5 member 6	8.21 ± 0.33	8.94 ± 0.23	Up	3.12 × 10 <sup>-3</sup>
<i>Slc1a5</i>	Solute carrier family 1 member 5	5.11 ± 0.36	6.15 ± 0.11	Up	3.27 × 10 <sup>-3</sup>
<i>Slc29a1</i>	Solute carrier family 29 member 1 (Augustine blood group)	7.76 ± 0.35	8.45 ± 0.08	Up	4.39 × 10 <sup>-3</sup>
<i>Slc6a6</i>	Solute carrier family 6 member 6	10.48 ± 0.58	11.31 ± 0.15	Up	6.05 × 10 <sup>-3</sup>
<i>Slc1a1</i>	Solute carrier family 1 member 1	10.59 ± 0.31	11.13 ± 0.13	Up	2.41 × 10 <sup>-2</sup>
<i>Slc44a1</i>	Solute carrier family 44 member 1	9.99 ± 0.2	10.44 ± 0.23	Up	4.07 × 10 <sup>-2</sup>
<i>Slc5a3</i>	Solute carrier family 5 member 3	9.50 ± 0.4	8.55 ± 0.37	Down	2.99 × 10 <sup>-4</sup>
<i>Tfrc</i>	Transferrin receptor	11.39 ± 0.29	10.63 ± 0.25	Down	1.29 × 10 <sup>-3</sup>
<i>Aqp4</i>	Aquaporin 4	11.83 ± 0.32	10.98 ± 0.51	Down	3.58 × 10 <sup>-3</sup>

bacterial LPS receptor TLR4 and its heterodimeric partner MD-2, including morphine-3-glucuronide,<sup>22</sup> ethyl glucuronide<sup>20</sup> and a range of steroid hormone glucuronide conjugates,<sup>21</sup> leading us to hypothesize that this may also be the case for pCG. LPS is known to circulate at low, but non-zero, levels in normal mice and humans,<sup>37,38</sup> and is known to enhance BBB permeability *in vitro* and *in vivo*<sup>10</sup>; hence, we investigated the interaction between it and pCG in our model system.

We initially confirmed that hCMEC/D3 cells express TLR4 and its accessory proteins MD-2 and CD14 (Suppl. Figure 3a-c). Treatment of hCMEC/D3 cells with LPS (*Porphyromonas gingivalis*, 10 ng/ml, 24 h) significantly enhanced paracellular permeability to a 70 kDa FITC-dextran tracer (Figure 4a) and reduced transendothelial electrical resistance (Figure 4b), effects that were both prevented by 30 minutes pre-treatment with pCG (1 μM). Similar treatment of endothelial monolayers with LPS disrupted circumferential localization of the key tight junction molecule ZO-1 (Figure 4c) and induced the appearance of large numbers of cytosolic actin fibers (Figure 4d), both of which features were prevented by 30 minutes pre-treatment with pCG (1 μM). This effect did

not appear to be due to down-regulation of TLR4 or its accessory molecules CD14 or MD-2 on the surface of the endothelial cells (Figure 4e-g), suggesting pCG may be acting as an antagonist at this receptor.

To provide further support for this hypothesis, we investigated whether pCG could functionally antagonize an alternative and unrelated effect of LPS treatment, upregulation of surface expression of the integrin CD11b on the human monocyte cell line THP-1 (Suppl. Figure 3). Treatment of THP-1 cells with LPS (20 ng/ml, 24 h) significantly upregulated surface CD11b expression, an effect prevented by 30 minutes pre-treatment with 1 μM pCG (Figure 4g), confirming the ability of pCG to antagonize LPS-induced signaling responses in distinct circumstances.

## Discussion

Glucuronidation is a key stage in phase II metabolism and clearance of endogenous and exogenous molecules and has long been investigated in this regard. Much is now known about the various UDP-glucuronosyltransferases responsible for glucuronidation at different sites in the body,<sup>19</sup> but the

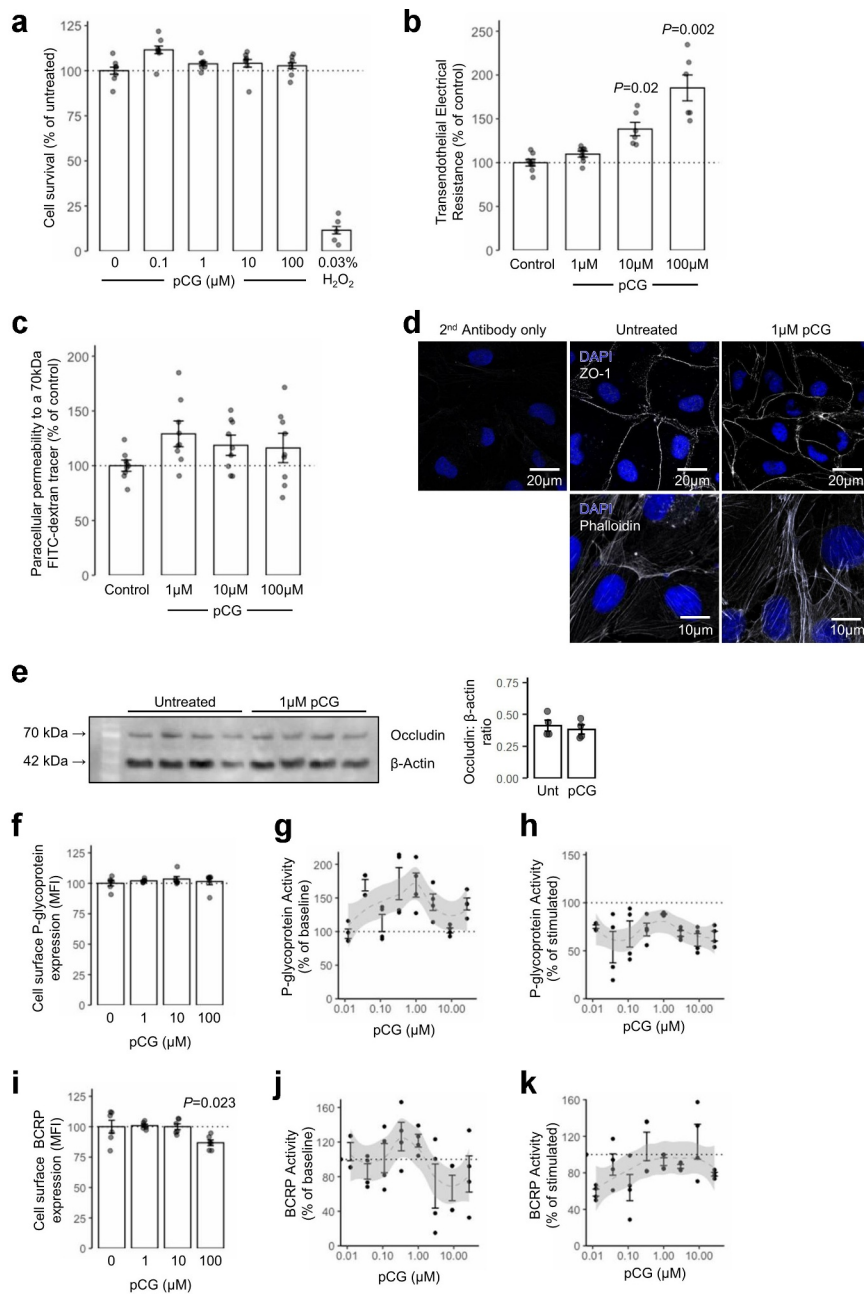


**Figure 3. Limited effects of pCG upon unstimulated *in vitro* models of the BBB.** (a) Treatment of hCMEC/D3 cells with increasing doses of pCG (0.1–100  $\mu\text{M}$ ; 24 h) has no effect on cell survival or proliferation as measured by the MTT assay, in contrast to the highly toxic effects of 0.03%  $\text{H}_2\text{O}_2$  exposure; data are mean  $\pm$  s.e.m.,  $n = 4$ . (b) Trans-endothelial electrical resistance across polarized hCMEC/D3 monolayers following 24 h treatment with pCG; data are mean  $\pm$  s.e.m.,  $n = 6$ . (c) Paracellular permeability of polarized hCMEC/D3 monolayers to a 70 kDa FITC-dextran tracer following 24 h treatment with pCG; data are mean  $\pm$  s.e.m.,  $n = 9$ . (d) Confocal microscopic analysis of expression of the tight junction component zona occludens-1 (ZO-1) or AF488-phalloidin labeled actin filaments in hCMEC/D3 cells following treatment for 24 h with 1  $\mu\text{M}$  pCG. Images are representative of at least three independent experiments. (e) Treatment of hCMEC/D3 cells with 1  $\mu\text{M}$  pCG (24 h) had no effect on total occludin expression; quantified data are mean integrated optical densities  $\pm$  s.e.m.,  $n = 4$ . (f) Treatment of hCMEC/D3 cells with pCG (24 h) had no effect on cell surface expression of P-glycoprotein, data are mean  $\pm$  s.e.m.,  $n = 6$ . (G, H) Lack of stimulatory (f) or inhibitory (g) effects of pCG upon baseline or stimulated P-glycoprotein activity, data are mean  $\pm$  s.e.m.,  $n = 4$ . (I) Treatment of hCMEC/D3 cells with pCG (24 h) caused a slight but significant reduction in BCRP expression at the highest dose tested (100  $\mu\text{M}$ ), data are mean  $\pm$  s.e.m.,  $n = 6$ . (J, K) Lack of stimulatory (i) or inhibitory (j) effects of pCG upon baseline or stimulated BCRP activity, data are mean  $\pm$  s.e.m.,  $n = 4$ .

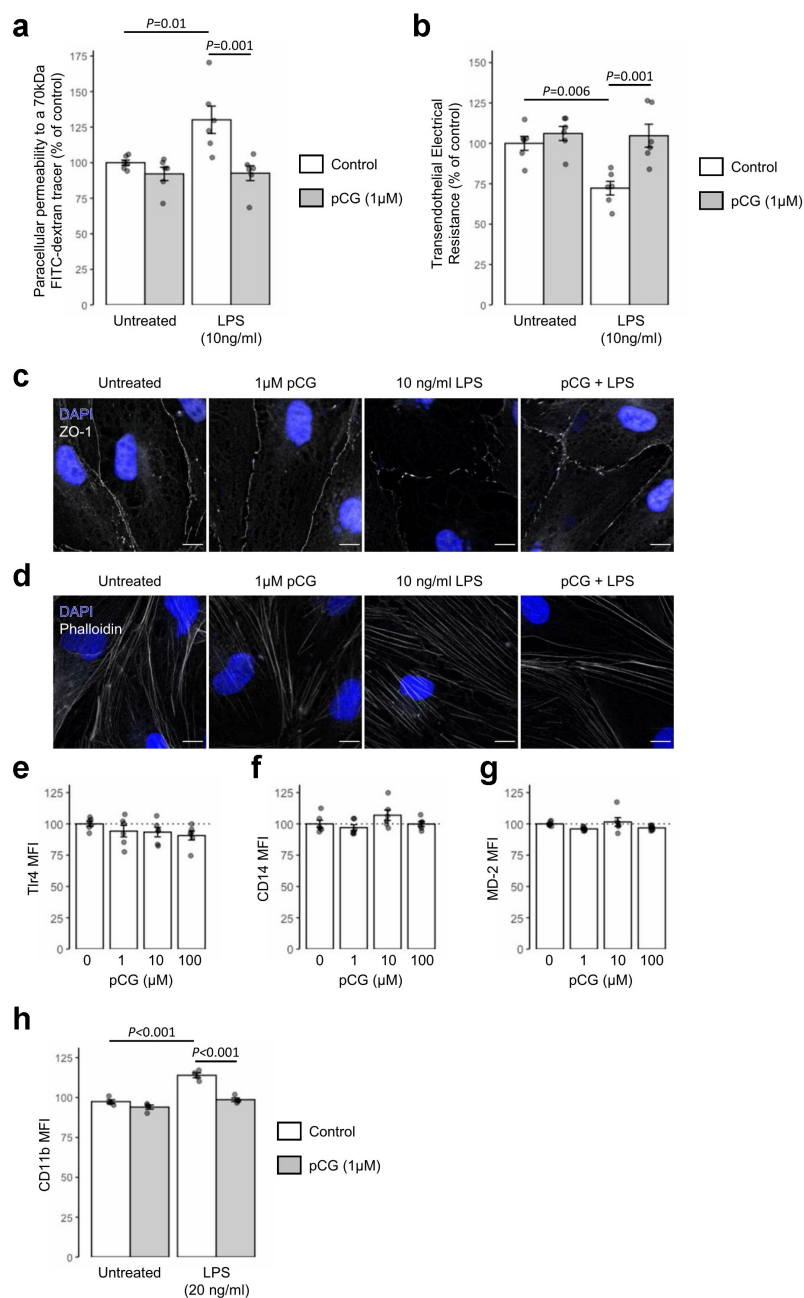


**Figure 4. Treatment with pCG antagonizes the effects of LPS in vitro.** (a) Paracellular permeability of polarized hCMEC/D3 monolayers to a 70 kDa FITC-dextran tracer with or without 24 h treatment with *Porphyromonas gingivalis* LPS (10 ng/ml) under control conditions or with 30 minutes pre-treatment with 1  $\mu$ M pCG; data are mean  $\pm$  s.e.m.,  $n = 6$ . (b) Transendothelial electrical resistance of polarized hCMEC/D3 monolayers to a 70 kDa FITC-dextran tracer with or without 24 h treatment with *P. gingivalis* LPS (10 ng/ml) under control conditions or with 30 minutes pretreatment with 1  $\mu$ M pCG; data are mean  $\pm$  s.e.m.,  $n = 6$ . (c) Confocal microscopic analysis of expression of the tight junction component zona occludens-1 (ZO-1) in hCMEC/D3 cells following treatment for 24 h with 10 ng/ml LPS with or without 30 minutes prior administration of 1  $\mu$ M pCG. Images are representative of at least three independent experiments. (d) Confocal microscopic analysis of AF488-phalloidin defined actin filaments in hCMEC/D3 cells following treatment for 24 h with 10 ng/ml LPS with or without 30 minutes prior administration of 1  $\mu$ M pCG. Images are representative of at least three independent experiments. (e) Treatment of hCMEC/D3 cells with pCG (1–100  $\mu$ M, 24 h) has no effect on surface expression of TLR4; data are mean  $\pm$  s.e.m.,  $n = 6$ . (f) Treatment of hCMEC/D3 cells with pCG (1–100  $\mu$ M, 24 h) has no effect on surface expression of CD14; data are mean  $\pm$  s.e.m.,  $n = 6$ . (g) Treatment of hCMEC/D3 cells with pCG (1–100  $\mu$ M, 24 h) has no effect on surface expression of MD-2; data are mean  $\pm$  s.e.m.,  $n = 6$ . (h) Pre-treatment for 30 minutes with pCG (1  $\mu$ M) prevents the increase in cell surface CD11b expression on THP-1 monocyte-like cells induced by 24 h treatment with LPS (20 ng/ml); data are mean  $\pm$  s.e.m.,  $n = 4$ .

biological actions of glucuronide compounds once they have been formed are rather less understood. In most cases, glucuronide conjugates have been considered as biologically inactive and simply destined for renal elimination, but our data add to the steadily building picture that this may not be universally true. Notably, glucuronide derivatives of morphine, ethanol and estradiol have been shown to act as agonists of the TLR4 complex, promoting allodynia and inflammation upon spinal cord administration.<sup>20–22</sup> Our data add the tyrosine/phenylalanine metabolite pCG to the list of glucuronide conjugates that can interact with TLR4 signaling, but with the marked difference that, in contrast to the other known activating agents, pCG is a functional antagonist and prevents the permeabilizing effects of bacterial endotoxin exposure upon the BBB.

While pCG has long been known to circulate in the blood, its physiological and potentially pathological actions have remained somewhat elusive. Our description of an antagonistic action of pCG upon the principal LPS receptor, the TLR4 complex, indicates an anti-inflammatory effect of the molecule and suggests that it may, at least at physiological concentrations, aid cerebrovascular resilience to the damaging effects of LPS exposure,<sup>33,39</sup> thereby protecting against the development of sickness behaviors.<sup>40</sup> However, pCG is also well known as a potential uremic toxin.<sup>41</sup> Exposure at levels seen in patients undergoing hemodialysis has been reported to directly evoke a low level of endothelial reactive oxygen species release,<sup>42</sup> to impair endothelial succinate dehydrogenase function<sup>43</sup> and to potentiate some of the inflammatory effects of pCS upon leukocytes<sup>17</sup> and the endothelium.<sup>44</sup> Notably, individuals with renal dysfunction have increased susceptibility to bacterial infection<sup>45–47</sup> despite the presence of chronic low-grade leukocyte activation.<sup>48</sup> Given that the majority of circulating pCG in such patients is freely available<sup>49</sup> and thus presumably able to interact with TLR4, the potential contribution that such antagonism by pCG makes to masking signs of bacterial infection bears further investigation.

Beyond emphasizing the need to look again at glucuronide conjugates as potential biological actors, our data also highlight the position of the cerebral vasculature and the BBB as targets for the actions of microbial metabolites and an important aspect of the gut–brain axis. A range of gut microbe-derived metabolites, including short-chain fatty acids, methylamines and, here, cresols, have now been shown to regulate BBB integrity<sup>9,10,29</sup> *in vivo*. That such structurally diverse molecules can modulate BBB function epitomizes the complexity of the gut microbiome–brain axis, but also emphasizes the importance of systematic investigation of this communication pathway. Moreover, as pCG is a product of both gut microbial and host enzymatic co-metabolism of aromatic amino acids, our data emphasize the need to consider both microbial and host systems in regulating gut microbe–brain communication. With over 200 known microbe-derived metabolites present in the human circulation,<sup>50</sup> there is clearly much still to learn about how they might influence the cerebral vasculature and their implications for health, aging and disease.

A notable feature of the gut microbiota is its exquisite sensitivity to dietary change,<sup>51</sup> with the makeup of the gut microbiome changing in a matter of weeks of exposure to a novel diet.<sup>52</sup> As diet is also known to be a major risk factor for cerebrovascular and neurological health,<sup>53</sup> studying the links between diet, gut microbe–host co-metabolites and the BBB may be instructive in understanding the pathogenesis of and, potentially, treatment for neurovascular disease. In particular, our study of the simple phenolic glucuronide pCG may be of relevance when it comes to understanding the actions of its more chemically complex relatives, the dietary polyphenol glucuronides. Diets supplemented with foods containing polyphenols have been shown to improve cerebral blood flow and neurovascular coupling in humans,<sup>54–58</sup> and rodent studies have revealed polyphenols to protect against ischemia or trauma-induced BBB integrity damage.<sup>59–62</sup> Notably, however, such dietary polyphenols are primarily found in the circulation as conjugates: sulfates, methylates, and, conspicuously, glucuronides.<sup>63</sup> At the least, the presence of high levels of glucuronide conjugates suggest that

these agents should be investigated as potential mediators of the beneficial effects of dietary polyphenols upon the cerebral vasculature.

## Conclusion

Here, we show that pCG, thought to be a relatively inert product of gut microbe–host enzyme co-metabolism, can influence the BBB and potentially immune cell activity through functional antagonism at the TLR4 complex. Notably, pCG administered within its physiological range was active *in vivo*, enhancing permeability barrier function of the cerebrovascular endothelium and further inducing significant transcriptional change throughout the brain. These findings extend our understanding of the role of glucuronide conjugates as not only targets for renal elimination but also as potent biological actors in their own right. Moreover, our data emphasize the importance of considering both microbial and host metabolic processes in understanding the mechanism(s) of communication that underlie the gut microbiota–brain axis.

## Statements and declarations

The authors have no competing interests to declare that are relevant to the content of this article. Author Contributions: AVS prepared and purified pCG, TBAK, SNS and SM performed cell culture and animal experiments, LH performed bioinformatic analyses. AVS, LH and SM wrote the manuscript. All authors have read and approved the final version of the manuscript.

## Acknowledgments

This work was funded by Alzheimer's Research UK Pilot Grant No. ARUK-PPG2016B-6. PREDEASY™ efflux transporter analysis kits were generously provided through the SOLVO Biotechnology Research and Academic Collaborative Transporter Studies (ReACTS) Program. This work used the computing resources of the UK MEDical BIOinformatics partnership—aggregation, integration, visualization and analysis of large, complex data (UK MED-BIO), which was supported by the Medical Research Council (grant number MR/L01632X/1). This project has received funding from the European Union's Horizon 2020 research and innovation program under grant agreement No 874583. This publication

reflects only the authors' view and the European Commission is not responsible for any use that may be made of the information it contains.

## Disclosure statement

No potential conflict of interest was reported by the author(s).

## Funding

This work was supported by the Horizon 2020 Framework Programme [874583]; Medical Research Council [MR/L01632X/1]; and Alzheimer's Research UK [ARUK-PPG2016B-6].

## ORCID

Simon McArthur  <http://orcid.org/0000-0001-8521-1808>

## References

1. Tang WHW, Kitai T, Hazen SL. Gut microbiota in cardiovascular health and disease. *Circ Res.* 2017;120:1183–1196. doi:10.1161/CIRCRESAHA.117.309715.
2. Hoyles L, Fernández-Real JM, Federici M, Serino M, Abbott J, Charpentier J, Heymes C, Luque JL, Anthony E, Barton RH, et al. Molecular phenomics and metagenomics of hepatic steatosis in non-diabetic obese women. *Nat Med.* 2018;24:1070–1080. doi:10.1038/s41591-018-0061-3.
3. Cheng WY, Wu CY, Yu J. The role of gut microbiota in cancer treatment: friend or foe? *Gut.* 2020;69:1867–1876. doi:10.1136/gutjnl-2020-321153.
4. Yuan X, Chen B, Duan Z, Xia Z, Ding Y, Chen T, Liu H, Wang B, Yang B, Wang X, et al. Depression and anxiety in patients with active ulcerative colitis: crosstalk of gut microbiota, metabolomics and proteomics. *Gut Microbes.* 2021;13:1987779. doi:10.1080/19490976.2021.1987779.
5. Leclercq S, Le Roy T, Furguele S, Coste V, Bindels LB, Leyrolle Q, Neyrinck AM, Quoilin C, Amadieu C, Petit G, et al. Gut microbiota-induced changes in  $\beta$ -hydroxybutyrate metabolism are linked to altered sociability and depression in alcohol use disorder. *Cell Rep.* 2020;33:108238. doi:10.1016/j.celrep.2020.108238.
6. van Kessel Sp, Frye AK, El-Gendy AO, Castejon M, Keshavarzian A, van Dijk G, El Aidy S, van Kessel SP. Gut bacterial tyrosine decarboxylases restrict levels of levodopa in the treatment of Parkinson's disease. *Nat Commun.* 2019;10:1–11. doi:10.1038/s41467-019-08294-y.
7. Rothhammer V, Mascanfroni ID, Bunse L, Takenaka MC, Kenison JE, Mayo L, Chao CC, Patel B, Yan R, Blain M, et al. Type I interferons and microbial metabolites of



- tryptophan modulate astrocyte activity and central nervous system inflammation via the aryl hydrocarbon receptor. *Nat Med.* 2016;22:586–597. doi:10.1038/nm.4106.
8. Marizzoni M, Cattaneo A, Mirabelli P, Festari C, Lopizzo N, Nicolosi V, Mombelli E, Mazzelli M, Luongo D, Naviglio D, et al. Short-chain fatty acids and lipopolysaccharide as mediators between gut dysbiosis and amyloid pathology in Alzheimer's disease. *J Alzheimer's Dis.* 2020;78:683–697. doi:10.3233/JAD-200306.
  9. Braniste V, Al-Asmakh M, Kowal C, Anuar F, Abbaspour A, Tóth M, Korecka A, Bakocevic N, Guan NL, Kundu P, et al. The gut microbiota influences blood-brain barrier permeability in mice. *Sci Transl Med.* 2014;6:263ra158–263ra158. doi:10.1126/scitranslmed.3009759.
  10. Hoyles L, Pontifex MG, Rodriguez-Ramiro I, Anis-Alavi MA, Jelane KS, Snelling T, Solito E, Fonseca S, Carvalho AL, Carding SR, et al. Regulation of blood–brain barrier integrity by microbiome-associated methylamines and cognition by trimethylamine N-oxide. *Microbiome.* 2021;9:235. doi:10.1186/s40168-021-01181-z.
  11. Saito Y, Sato T, Nomoto K, Tsuji H. Identification of phenol- and p-cresol-producing intestinal bacteria by using media supplemented with tyrosine and its metabolites. *FEMS Microbiol Ecol.* 2018;94:125. doi:10.1093/femsec/fiy125.
  12. Ramakrishna BS, Gee D, Weiss A, Pannall P, Roberts-Thomson IC, Roediger WEW. Estimation of phenolic conjugation by colonic mucosa. *J Clin Pathol.* 1989;42:620–623. doi:10.1136/jcp.42.6.620.
  13. Rong Y, Kiang TKL. Characterizations of human UDP-glucuronosyltransferase enzymes in the conjugation of p-cresol. *Toxicol Sci.* 2020;176:285–296. doi:10.1093/toxsci/kfaa072.
  14. Vanholder R, Bammens B, De Loor H, Glorieux G, Meijers B, Schepers E, Massy Z, Evenepoel, Evenepoel P. The unfortunate end of p-cresol as a uraemic toxin. *Nephrol Dial Transplant.* 2011;26:1464–1467. doi:10.1093/ndt/gfr056.
  15. Gryp T, Vanholder R, Vanechoutte M, Glorieux G. P-Cresyl Sulfate. *Toxins (Basel).* 2017;9:52. doi:10.3390/toxins9020052.
  16. Vanholder R, De Smet R, Lesaffer G. p-Cresol: a toxin revealing many neglected but relevant aspects of uraemic toxicity. *Nephrol Dial Transplant.* 1999;14:2813–2815. doi:10.1093/ndt/14.12.2813.
  17. Meert N, Schepers E, Glorieux G, Van Landschoot M, Goeman JL, Waterloos MA, Dhondt A, Van Der Eycken J, Vanholder R. Novel method for simultaneous determination of p-cresylsulphate and p-cresylglucuronide: clinical data and pathophysiological implications. *Nephrol Dial Transplant.* 2012;27:2388–2396. doi:10.1093/ndt/gfr672.
  18. Koppe L, Alix PM, Croze ML, Chambert S, Vanholder R, Glorieux G, Fouque D, Soulage CO. P-Cresyl glucuronide is a major metabolite of p-cresol in mouse: in contrast to p-cresyl sulphate, p-cresyl glucuronide fails to promote insulin resistance. *Nephrol Dial Transplant.* 2017;32:2000–2009. doi:10.1093/ndt/gfx089.
  19. Yang N, Sun R, Liao X, Aa J, Wang G. UDP-glucuronosyltransferases (UGTs) and their related metabolic cross-talk with internal homeostasis: a systematic review of UGT isoforms for precision medicine. *Pharmacol Res.* 2017;121:169–183. doi:10.1016/j.phrs.2017.05.001.
  20. Lewis SS, Hutchinson MR, Zhang Y, Hund DK, Maier SF, Rice KC, Watkins LR. Glucuronic acid and the ethanol metabolite ethyl-glucuronide cause toll-like receptor 4 activation and enhanced pain. *Brain Behav Immun.* 2013;30:24–32. doi:10.1016/j.bbi.2013.01.005.
  21. Lewis SS, Hutchinson MR, Frick MM, Zhang Y, Maier SF, Sammakia T, Rice KC, Watkins LR. Select steroid hormone glucuronide metabolites can cause toll-like receptor 4 activation and enhanced pain. *Brain Behav Immun.* 2015;44:128–136. doi:10.1016/j.bbi.2014.09.004.
  22. Lewis SS, Hutchinson MR, Rezvani N, Loram LC, Zhang Y, Maier SF, Rice KC, Watkins LR. Evidence that intrathecal morphine-3-glucuronide may cause pain enhancement via toll-like receptor 4/MD-2 and interleukin-1 $\beta$ . *Neuroscience.* 2010;165:569–583. doi:10.1016/j.neuroscience.2009.10.011.
  23. Klimas R, Mikus G. Morphine-6-glucuronide is responsible for the analgesic effect after morphine administration: a quantitative review of morphine, morphine-6-glucuronide, and morphine-3-glucuronide. *Br J Anaesth.* 2014;113:935–944. doi:10.1093/bja/aeu186.
  24. London JA, Wang ECS, Barsukov IL, Yates EA, Stachulski AV. Synthesis and toxicity profile in 293 human embryonic kidney cells of the  $\beta$  D-glucuronide derivatives of ortho-, meta- and para-cresol. *Carbohydr Res.* 2021;499:108225–108230. doi:10.1016/j.carres.2020.108225.
  25. Love MI, Huber W, Anders S. Moderated estimation of fold change and dispersion for RNA-seq data with DESeq2. *Genome Biol.* 2014;15:550. doi:10.1186/s13059-014-0550-8.
  26. Chen EY, Tan CM, Kou Y, Duan Q, Wang Z, Meirelles GV, Clark NR, Ma'ayan A. Enrichr: interactive and collaborative HTML5 gene list enrichment analysis tool. *BMC Bioinform.* 2013;14:128. doi:10.1186/1471-2105-14-128.
  27. Kuleshov VM, Jones MR, Rouillard AD, Fernandez NF, Duan Q, Wang Z, Koplev S, Jenkins SL, Jagodnik KM, Lachmann A, et al. Enrichr: a comprehensive gene set enrichment analysis web server 2016 update. *Nucleic Acids Res.* 2016;44:W90–7. doi:10.1093/nar/gkw377.
  28. Tarca AL, Draghici S, Khatri P, Hassan SS, Mittal P, Kim J-S, Kim CJ, Kusanovic JP, Romero R. A novel signaling pathway impact analysis. *Bioinformatics.* 2009;25:75–82. doi:10.1093/bioinformatics/btn577.

29. Hoyles L, Snelling T, Umlai UK, Nicholson JK, Carding SR, Glen RC, McArthur S. Microbiome–host systems interactions: protective effects of propionate upon the blood–brain barrier. *Microbiome*. 2018;6:55. doi:10.1186/s40168-018-0439-y.
30. Weksler BB, Subileau EA, Perrière N, Charneau P, Holloway K, Leveque M, Tricoire-Leignel H, Nicotra A, Bourdoulous S, Turowski P, et al. Blood-brain barrier-specific properties of a human adult brain endothelial cell line. *FASEB J*. 2005;19:1872–1874. doi:10.1096/fj.04-3458fj.
31. Abbott NJ, Hughes CCW, Revest PA, Greenwood J. Development and characterisation of a rat brain capillary endothelial culture: towards an in vitro blood-brain barrier. *J Cell Sci*. 1992;103:23–37. doi:10.1242/jcs.103.1.23.
32. Coisne C, Dehouck L, Faveeuw C, Delplace Y, Miller F, Landry C, Morissette C, Fenart L, Cecchelli R, Tremblay P, et al. Mouse syngenic in vitro blood-brain barrier model: a new tool to examine inflammatory events in cerebral endothelium. *Lab Invest*. 2005;85:734–746. doi:10.1038/labinvest.3700281.
33. Maggioli E, McArthur S, Mauro C, Kieswich J, Kusters DHM, Reutelingsperger CPM, Yaqoob M, Solito E. Estrogen protects the blood–brain barrier from inflammation-induced disruption and increased lymphocyte trafficking. *Brain Behav Immun*. 2016;51:212–222. doi:10.1016/j.bbi.2015.08.020.
34. Xie Z, Bailey A, Kuleshov MV, Clarke DJB, Evangelista JE, Jenkins SL, Lachmann A, Wojciechowicz ML, Kropiwnicki E, Jagodnik KM, et al. Gene set knowledge discovery with enrichr. *Curr Protoc*. 2021;1:e90. doi:10.1002/cpz1.90.
35. Weksler B, Romero IA, Couraud P-O. The hCMEC/D3 cell line as a model of the human blood brain barrier. *Fluids Barriers CNS*. 2013;10:16. doi:10.1186/2045-8118-10-16.
36. Sjöstedt E, Zhong W, Fagerberg L, Karlsson M, Mitsios N, Adori C, Oksvold P, Edfors F, Limiszewska A, Hikmet F, et al. An atlas of the protein-coding genes in the human, pig, and mouse brain. *Science* (80-). 2020;367:eaay5947. doi:10.1126/science.aay5947.
37. Wiedermann CJ, Kiechl S, Dunzendorfer S, Schratzberger P, Egger G, Oberhollenzer F, Willeit J. Association of endotoxemia with carotid atherosclerosis and cardiovascular disease: prospective results from the Bruneck study. *J Am Coll Cardiol*. 1999;34:1975–1981. doi:10.1016/S0735-1097(99)00448-9.
38. Cani PD, Amar J, Iglesias MA, Poggi M, Knauf C, Bastelica D, Neyrinck AM, Fava F, Tuohy KM, Chabo C, et al. Metabolic endotoxemia initiates obesity and insulin resistance. *Diabetes*. 2007;56:1761–1772. doi:10.2337/db06-1491.
39. Brezzo G, Simpson J, Ameen-Ali KE, Berwick J, Martin C. Acute effects of systemic inflammation upon the neuro-glial-vascular unit and cerebrovascular function. *Brain, Behav Immun - Heal*. 2020;5:100074. doi:10.1016/j.bbih.2020.100074.
40. Schedlowski M, Engler H, Grigoleit JS. Endotoxin-induced experimental systemic inflammation in humans: a model to disentangle immune-to-brain communication. *Brain Behav Immun*. 2014;35:1–8. doi:10.1016/j.bbi.2013.09.015.
41. Liabeuf S, Glorieux G, Lenglet A, Diouf M, Schepers E, Desjardins L, Choukroun G, Vanholder R, Massy ZA. Does P-cresylglucuronide have the same impact on mortality as other protein-bound uremic toxins?. *PLoS One*. 2013;8(6):e67168–e67178. doi:10.1371/journal.pone.0067168.
42. Itoh Y, Ezawa A, Kikuchi K, Tsuruta Y, Niwa T. Protein-bound uremic toxins in hemodialysis patients measured by liquid chromatography/tandem mass spectrometry and their effects on endothelial ROS production. *Anal Bioanal Chem*. 2012;403:1841–1850. doi:10.1007/s00216-012-5929-3.
43. Mutsaers HAM, Wilmer MJG, Reijnders D, Jansen J, van den Broek PHH, Forkink M, Schepers E, Glorieux G, Vanholder R, van den Heuvel LP, et al. Uremic toxins inhibit renal metabolic capacity through interference with glucuronidation and mitochondrial respiration. *Biochim Biophys Acta - Mol Basis Dis*. 2013;1832:142–150. doi:10.1016/j.bbadis.2012.09.006.
44. Pletinck A, Glorieux G, Schepers E, Cohen G, Gondouin B, Van Landschoot M, Eloit S, Rops A, Van De Voorde J, De Vriese A, et al. Protein-bound uremic toxins stimulate crosstalk between leukocytes and vessel wall. *J Am Soc Nephrol*. 2013;24:1981–1994. doi:10.1681/ASN.2012030281.
45. Sarnak MJ, Jaber BL. Mortality caused by sepsis in patients with end-stage renal disease compared with the general population. *Kidney Int*. 2000;58:1758–1764. doi:10.1111/j.1523-1755.2000.00337.x.
46. Ishigami J, Grams ME, Chang AR, Carrero JJ, Coresh J, Matsushita K. CKD and risk for hospitalization with infection: the Atherosclerosis risk in communities (ARIC) study. *Am J Kidney Dis*. 2017;69:752–761. doi:10.1053/j.ajkd.2016.09.018.
47. Thompson S, James M, Wiebe N, Hemmelgarn B, Manns B, Klarenbach S, Tonelli M. Cause of death in patients with reduced kidney function. *J Am Soc Nephrol*. 2015;26:2504–2511. doi:10.1681/ASN.2014070714.
48. Espi M, Koppe L, Fouque D, Thauinat O. Chronic kidney disease-associated immune dysfunctions: impact of protein-bound uremic retention solutes on immune cells. *Toxins (Basel)*. 2020;12:300. doi:10.3390/toxins12050300.

49. Yi D, Monteiro EB, Chambert S, Soula HA, Daleprane JB, Soulage CO. Determination of the binding properties of p-cresyl glucuronide to human serum albumin. *Biochimie*. 2018;150:1–7. doi:10.1016/j.biochi.2018.04.019.
50. Russell WR, Hoyles L, Flint HJ, Dumas M-E. Colonic bacterial metabolites and human health. *Curr Opin Microbiol*. 2013;16:246–254. doi:10.1016/j.mib.2013.07.002.
51. Wolter M, Grant ET, Boudaud M, Steimle A, Pereira GV, Martens EC, Desai MS. Leveraging diet to engineer the gut microbiome. *Nat Rev Gastroenterol Hepatol*. 2021;18:885–902. doi:10.1038/s41575-021-00512-7.
52. David LA, Maurice CF, Carmody RN, Gootenberg DB, Button JE, Wolfe BE, Ling AV, Devlin AS, Varma Y, Fischbach MA, et al. Diet rapidly and reproducibly alters the human gut microbiome. *Nature*. 2014;505:559–563. doi:10.1038/nature12820.
53. Jackson PA, Pialoux V, Corbett D, Drogos L, Erickson KI, Eskes GA, Poulin MJ. Promoting brain health through exercise and diet in older adults: a physiological perspective. *J Physiol*. 2016;594:4485–4498. doi:10.1113/JP271270.
54. Lamport DJ, Pal D, Macready AL, Barbosa-Boucas S, Fletcher JM, Williams CM, Spencer JPE, Butler LT. The effects of flavanone-rich citrus juice on cognitive function and cerebral blood flow: an acute, randomised, placebo-controlled cross-over trial in healthy, young adults. *Br J Nutr*. 2016;116:2160–2168. doi:10.1017/S000711451600430X.
55. Liu R, Zhang TT, Zhou D, Bai XY, Zhou WL, Huang C, Song JK, Meng FR, Wu CX, Li L, et al. Quercetin protects against the A $\beta$ 25–35-induced amnesic injury: involvement of inactivation of RAGE-mediated pathway and conservation of the NVU. *Neuropharmacology*. 2013;67:419–431. doi:10.1016/j.neuropharm.2012.11.018.
56. Schroeter H, Heiss C, Balzer J, Kleinbongard P, Keen CL, Hollenberg NK, Sies H, Kwik-Urbe C, Schmitz HH, Kelm M. (-)-Epicatechin mediates beneficial effects of flavanol-rich cocoa on vascular function in humans. *Proc Natl Acad Sci U S A*. 2006;103:1024–1029. doi:10.1073/pnas.0510168103.
57. Squadrito F, Altavilla D, Morabito N, Crisafulli A, D’Anna R, Corrado F, Ruggeri P, Campo GM, Calapai G, Caputi AP, et al. The effect of the phytoestrogen genistein on plasma nitric oxide concentrations, endothelin-1 levels and endothelium dependent vasodilation in postmenopausal women. *Atherosclerosis*. 2002;163:339–347. doi:10.1016/S0021-9150(02)00013-8.
58. Thaug Zaw JJ, Howe PRC, Wong RHX. Sustained cerebrovascular and cognitive benefits of resveratrol in postmenopausal women. *Nutrients*. 2020;12(3):828–842. doi:10.3390/nu12030828.
59. Hong G, Yan Y, Zhong Y, Chen J, Tong F, Ma Q. Combined ischemic preconditioning and resveratrol improved bloodbrain barrier breakdown via Hippo/YAP/TAZ signaling pathway. *CNS Neurol Disord - Drug Targets*. 2019;18:713–722. doi:10.2174/1871527318666191021144126.
60. Liu R, Xinming Z, Jing Z, Zhihua H, Li X, Xiao H, Chen Q, Li D. 3'-Daidzein sulfonate sodium inhibits neuronal apoptosis induced by cerebral ischemia-reperfusion. *Int J Mol Med*. 2017;39:1021–1028. doi:10.3892/ijmm.2017.2915.
61. Jiang Z, Zhang J, Cai Y, Huang J, You L. Catechin attenuates traumatic brain injury-induced blood–brain barrier damage and improves longer-term neurological outcomes in rats. *Exp Physiol*. 2017;102:1269–1277. doi:10.1113/EP086520.
62. Soltani Z, Khaksari M, Jafari E, Iranpour M, Shahrokhi N. Is genistein neuroprotective in traumatic brain injury? *Physiol Behav*. 2015;152:26–31. doi:10.1016/j.physbeh.2015.08.037.
63. Manach C, Scalbert A, Morand C, Rémésy C, Jiménez L. Polyphenols: food sources and bioavailability. *Am J Clin Nutr*. 2004;79:727–747. doi:10.1093/ajcn/79.5.727.